Impurity diffusion induced dynamic electron donors in semiconductors

Wen-Hao Liu, Jun-Wei Luo, Shu-Shen Li, and Lin-Wang Wang

Phys. Rev. B **100**, 165203 — Published 22 October 2019

DOI: 10.1103/PhysRevB.100.165203

Impurity diffusion induced dynamic electron donor in semiconductors

Wen-Hao Liu[1,2], Jun-Wei Luo[1,2,3]*, Shu-Shen Li[1,2,3], and Lin-Wang Wang[4]*

[1]*State Key Laboratory of Superlattices and Microstructures, Institute of Semiconductors, Chinese Academy of Sciences, Beijing 100083, China*

[2]*Center of Materials Science and Optoelectronics Engineering, University of Chinese Academy of Sciences, Beijing 100049, China*

[3]*Beijing Academy of Quantum Information Sciences, Beijing 100193, China*

[4]*Materials Science Division, Lawrence Berkeley National Laboratory, Berkeley, California 94720, United States*

*Email: jwluo@semi.ac.cn; lwwang@lbl.gov

Abstract:

Low energy impurity diffusion in a host material is often regarded as an adiabatic process, characterized by its adiabatic potential energy barrier. Here, we show that the diffusion process in semiconductors can involve nonadiabatic electron excitations, rending it to be a more complicated process. Impurity diffusion in a device at working temperature can pump one electron up from localized impurity state into the host conduction band and causes the impurity to be a dynamic donor since it temporarily loses its electron to the host. This nonadiabatic process, against a common belief, fundamentally change the diffusion behavior, including its barrier height and diffusion path. Although we mainly demonstrate this process with Au metal impurity in bulk Si through time-dependent density functional theory simulations, we believe this could be a rather common phenomenon as it is shown that the similar phenomena also exist in Zn, Cd impurities diffusion in bulk Si, and Ti diffusion in TiO_2. We believe this study can open up a new direction of inquiry for such diffusion behavior in semiconductor.

Nonadiabatic coupling of nuclear motion to electronic excitations has recently been recognized in many chemical reactions [1-8] and radiation processes [9-18] in a wide range of material systems, attracting a great deal of experimental and theoretical interest. Although the collision of high energy ions with a host material is a well-recognized nonadiabatic process [9,18], recent studies show that nonadiabatic process can also occur in relatively low energy reactions [1-18], e.g., the catalytic molecule dissociation [3,6]. Impurity diffusion is one of the most fundamental processes in semiconductor systems. Not only it is relevant for device reliability, it is also essential during synthesis. For example, controlled incorporation of extrinsic impurity in semiconductors requires a deep understanding of the atomistic mechanisms of the diffusion path. As a long-standing topic, extensive studies have been devoted to understand impurity diffusion in semiconductors, with special emphasis on the diffusion path, barrier height. It has long been believed this is a well understood problem, except perhaps for some coordinated movements, with a classical nuclei movement picture based on adiabatic ground states for the electronic structures [19,20]. Similarly, the charging state of an impurity has often been understood, and theoretically calculated, as a ground state energy problem. There are rarely any considerations for the possibility that its charge state can change during the diffusion process.

In this letter, we reveal that, surprisingly, the thermally activated impurity diffusion in semiconductors can often be a nonadiabatic process, which pumps an electron from a localized impurity state inside the host band gap into the host conduction band, and hence makes it dynamically a positively charged donor for an otherwise neutral impurity. This will render the impurity as a positively charge state during the critical diffusion process, thus different from the common ground state impurity charge state calculation results. Such “dynamic donor” behavior can result in fundamentally different diffusion path, barrier height, and potential energy surface (PES), and can resolve some of the long-standing puzzles, including why the experimentally measured activation energy is usually higher than the ground state based on barrier height calculations.

In this work, we carry out real-time time-dependent density functional theory (rt-TDDFT) simulations [21] based on the local density approximation (LDA) [22] within density functional theory (DFT) framework with a plane wave nonlocal pseudopotential Hamiltonian. The basis set

of plan wave functions is obtained by an energy cutoff of 50 Ry. To overcome the well-known DFT underestimation of the band gap (0.62 eV instead of 1.12 eV for Si), we have adjusted the s-state nonlocal pseudopotential to correct the Si band gap to the experimental value. Fortunately, this adjustment does not change the energy of occupied states and thus has a negligible effect on the total energy and the ground state dynamics of the investigated systems (details see supplemental note 1). [23] A 64 Si-atom periodic supercell is adopted to model the Si host crystal. Because conventional rt-TDDFT simulations are extreme expensive computationally, we utilize our newly developed rt-TDDFT algorithm [21] implemented in the code PWmat [24] to dramatically speed up the simulation [16,25,26] by increasing the time step from sub-attosecond to 0.1 femtosecond (fs). Hellman-Feynman forces is used in our newly developed rt-TDDFT . In order to cure the instabilities caused by the use of Hellman-Feynman forces, we have developed the new algorithm, which ensures the energy is conserved in a large time scale and increases the effective time step from <1 as in traditional methods to 0.1–0.5 fs. The adoption of this new algorithm enables us to simulate the system evolution in a picosecond (ps) within 24 hours in wall-clock time on a 4-GPU workstation which applies the architecture of Pascal GPU .

We note that the systems involving excitation of unpaired electrons have a multiplicity other than one spin configuration and thence possess an artificial mixture of spin states in spin-nonpolarized calculations. Such artificial spin-mixing gives rise to spin contamination since wavefunctions obtained from spin-nonpolarized calculations are no longer eigenfunctions of the total spin operator $\hat{S}^2$ [27]. Fortunately, spin contamination is less common to find any significant spin contamination in DFT calculations, even when spin-nonpolarized Kohn-Sham orbitals are being used [28]. Despite a correction due to spin contamination in the order of 10% was recently observed in the calculation of the TiO_2 bandgap utilizing a self-consistent field (ΔSCF) method within the DFT [29], and the spin-polarization maybe is an effective freedom in magnetic systems [30,31]. However, we find that the effect of the spin polarization will not affect our conclusion based on a detailed case of spin-polarized rt-TDDFT simulation (see note 5 in supplemental material). [23] We therefore carry out all calculations without considering spin-orbit coupling and spin-polarization in the text.

To simulate the low energy diffusion, the Au impurity is located at the tetrahedral interstitial

site (T-site) of the Si crystal at $t_0 = 0$ with an initial velocity $V_k = 6.642\times10^{-3}$ Å/fs (corresponding to a kinetic energy $E_k(t_0) = 0.45$ eV) moving toward the next T-site through the saddle point at the hexagonal interstitial site (H-site) along the <111> direction, as schematically illustrated in Fig. 1(a). The initial state of Au interstitial impurity and Si crystal have been relaxed at the most stable positions before the rt-TDDFT simulations. The initial temperature of the Si crystal is 550 K and Si crystal is allowed to move according to the Ehrenfest dynamics in rt-TDDFT simulation. This setting is to mimic the Au impurity diffusion occurring in the thermal diffusion or final stopping stage of the ion implantation in Si crystal. The diffusivity of an impurity is usually quantified by an energy barrier E_b (also called activation energy) on PES [32], which, here, is the total energy difference of the system when the Au atom is at the H-site and at T-site. Figure 1(b) and (c) show the simulations of Au diffusion path in Si crystal up to 4 ps utilizing the Born–Oppenheimer Molecular Dynamics (BOMD) and rt-TDDFT methods, respectively. In the BOMD simulation, the Au atom travels from the T-site through the H-site to a next T-site, and then wanders around this next T-site (2.352 Å away from the initial T-site) as shown in Fig. 1(b), indicating successful hoping from one T-site to next T-site. Whereas, in the rt-TDDFT simulation, the Au atom travels in distance only up to 1.8 Å, then returns back and moves around the H-site (1.176 Å away from the initial T-site) as shown in Fig. 1(c). Their difference in diffusion behaviors is also indicated by the evolution of the Au kinetic energy. Figure 1(c) shows that both BOMD and rt-TDDFT simulations exhibit initially a similar reduction in the Au kinetic energy but substantially different after 0.3 ps. In BOMD simulation, after passing the H-site (the saddle point of the PES) at around 0.3 ps, the Au atom partially regains its kinetic energy with an amplitude close to the energy barrier E_b in the ground state as predicted by the nudge elastic band (NEB) method [33,34] as shown in Fig. 1(h). In contrast, the rt-TDDFT simulation exhibits that the Au atom continues to lose its kinetic energy.

To reveal the mechanism behind their difference, we examine the evolution of energy levels of adiabatic eigen states and their electron occupations in BOMD and rt-TDDFT simulations, as shown in Fig. 1(f) and (g), respectively. Accompanying the diffusion of the Au impurity, the low lying impurity state (level-1), which is occupied by one electron, lifts up in energy and the high lying unoccupied impurity state (level-2) shifts down, and their energy levels avoided cross when the Au atom passing the H-site. In the rt-TDDFT simulation, accompanying the anticrossing in these two levels, the electron initially occupied the level-1 is excite to the level-2 and then to the

host Si conduction band. Consequently, the system become excited instead of in its adiabatic ground state after Au passing the H-site, causing the impurity to be a dynamic donor since it temporarily loses its electron to the host. However, in the BOMD simulation, the impurity electron always occupies the low-lying impurity state in spite of anticrossing in two impurity levels. Regarding the nonadiabatic electron excitation makes the Au atom as Au^+ ion once it passes the H-site, we compare in Fig. 1(h) the ground state PES of both Au and Au^+ migration from T-site through H-site to next T-site in Si crystal using the NEB method. In the case of neutral Au atom, the PES minimum is at T-site, and the PES saddle point at H-site, giving rise to an energy barrier of E_b = 0.23 eV. Whereas, in the case of positively charged Au^+, the NEB method predicts that T-site is converted into the PES saddle point and the H-site becomes the PES minimum with a much smaller energy barrier of E_b = 0.07 eV. The reverse in the minimum and saddle points of the PES is responsible for the oscillation of the Au impurity around the H-site in rt-TDDFT simulation as shown in Fig. 1(b) and (c), since the Au atom effectively becomes Au^+ after 0.3 ps. Therefore, we could conclude that the striking difference is caused by the nonadiabatic excitation effect, an available feature in rt-TDDFT simulation but not in BOMD.

We continue the rt-TDDFT simulation to 4 ps, yet the excited electron is still in the host conduction band as shown in Fig. 1(g). Here, we have only used a 64 atom Si supercell for simulations. In reality, during this 4 ps, the electron diffusion distance will be 1.55×10^3 Å, much larger than the supercell we used, regarding the diffusion coefficient of Si electrons is nearly 10 cm^2/s for 500 K lattice temperature [35]. Consequently, the excited electron in fact will be lost to the host temporarily until it jumps down by thermal dynamic cooling which is probably in a time scale of ps [36]. We call this electron excitation phenomenon “dynamic donor”, which complicates the diffusion process and renders the conventional argument based on ground state barrier invalid. In the following, we examine the migration of the “dynamic donor” in comparison with the static donor diffusion in Si crystal.

Impurity diffusion in a semiconductor can be either in the form of a neutral atom or in the form of a charged ion. For instance, Cu diffusion in Si crystal in positively charged Cu^+ ion is well-documented. [37-40] As a matter of fact, the diffusion energy barrier of Cu atom (0.24 eV) is significantly reduced to the energy barrier of Cu^+ ion (0.18 eV), which is the smallest energy

barrier and responsible for the super diffusivity of Cu impurity [41] as the fastest diffusion impurity in Si. This situation has a natural explanation based on static DFT calculations. First-principles DFT predicts that the Cu^{+}/Cu^{0} transition level is above the conduction band minimum (CBM) of the Si host [42], indicating that the Cu^{+} is the ground state. Thus, even rest in Si crystal without moving, the Cu atom will be in the Cu^{+} state and become a static donor. The same is true for Li, Na, and K since their ground state is in the +1 ionic state in Si crystal. [43-46] However, this is not the case for other impurities, like Au, Cd, and Zn. Figure S2 [23] (see also references [47,48] therein) shows that first-principles DFT predicted transition levels of Au^{0}/Au^{+} Cd^{0}/Cd^{+}, and Zn^{0}/Zn^{+} are well below the host CBM, identifying them as the neutral impurity at ground states [49,50]. Nevertheless, their diffusion in Si crystal render them as "dynamic donor" as discussed above and shown in Supplementary Fig. S3. [23]

The electron excitation makes the "dynamic donor" diffusion process more complicated than the traditional adiabatic diffusion process. Specifically, due to the occurred energy transfer in the nonadiabatic electron excitation, the "dynamic donor" enhance the effective energy barrier over the ground state barrier predicted from the BOMD simulation, and more intriguingly, the diffusion distance does not even monotonically increase with the impurity initial velocity. Figure 2 shows the rt-TDDFT results with different initial kinetic energies of the Au impurity from 0.31 to 0.65 eV. Intricate behaviors are found in those rt-TDDFT simulations. First, in rt-TDDFT simulation, the Au did not reach the second T-site but returned to the initial T-site when the initial kinetic energy is 0.31 eV, which is higher than the energy barrier predicted directly from the BOMD simulation in the inset of Fig. 2(a) as well as the NEB calculated barrier (0.23 eV). This means the effective barrier in this nonadiabatic "dynamic donor" case is higher than the adiabatic barrier. Increase the Au initial kinetic energy to 0.35 eV in rt-TDDFT simulation, the Au went through the H-site, continued to pass next T- and H-sites, and was finally hovering between the third T-site and next H-site. We thus judge the effective energy barrier is between 0.31 eV and 0.35 eV (evaluated to be 0.33 eV), which is closer to the reported 0.39 eV of experimentally measured diffusion activation energy of Au in Si [51]. As we raise the initial kinetic energy to 0.55 eV and 0.65 eV, although the Au impurity passes the T-site, it retunes back and moves again around the H-site. Therefore, the diffusion of the "dynamic donor" is in sharp contrast to the conventional expectation where higher

in the initial kinetic energy is longer in diffuse distance. This anomalous behavior is a result of combination in the switch between the minimum and the saddle points in PES and energy transfer accompanying the loss in electron (>90%) from Au impurity to Si host as shown in Fig. 1(g). Whereas, in the lower kinetic energy cases (<0.35 eV), the impurity electron is not completely lost (e.g., in the 0.35 eV case, only 75% is lost) and energy transfer is less, that allows it to move further away. The loss of electron as a function of the Au velocity will be discussed below.

If "dynamic donor" phenomenon occurs for Au diffusion in Si, and thus the Au^+ barrier is as low as 0.07 eV in ground state as shown in Fig. 1(h), that mean whether the Au diffusion in Si is more fast. As mentioned above, the Au diffusion in Si has an experimentally measured activation energy of around 0.39 eV, even larger than the NEB calculated Au barrier of 0.23 eV, and also much larger than the Cu+ barrier of 0.18 eV [39,41]. Furthermore, the experimentally measured Cu diffusion constant is much larger than that of Au diffusion in Si [51]. The key rest on the fact, in most of the time, the Au should be in its neutral state at the T-site. The "dynamic donor" is only a transient phenomenon temporarily happen during the transition. Eventually, the electron will fall down to the impurity state (see Fig. S4). [23] As we show above, starting from the neutral Au atom, the nonadiabatic "dynamic donor" behavior can actually increase the barrier compared to the adiabatic counterpart. This might help to explain why the experimental activation energy is much higher than the NEB calculated one.

Next, we systematically investigate the effect of initial Au kinetic energy and the Si host crystal temperature on "dynamic donor" effect, more specifically to the amount of excited electrons transferred to the host conduction band. Figure 3(a) shows there are two Au impurity-induced defect states within the host Si band gap: when Au impurity locates at interstitial T-site, the low-lying occupied Au_i impurity state (level-1) is a single degenerate a_1 state derived purely from the Au 6*s* orbital, whereas, the high-lying unoccupied Au_i impurity state (level-2) is a three-fold degenerate t_2 state composed of Au 6*p* orbitals [50]. As Au impurity moving toward the H-site, change occurs in the symmetry of these two impurity states, causing state hybridization (Fig. S5) [23] since both of them belong to a_1 symmetry. As can been seen, the energy curves of two impurity levels form avoid crossing with an avoid-crossing gap Δ when the Au impurity is at the H-site. Consequently, the nonadiabatic excitation of electrons undergoing in rt-TDDFT

simulations can be described by Landau-Zener transition (LZT) [52] model for the transition probability in two-level system, where the transition probability p_{LZT}, corresponding to the amount of "dynamic donor" excitation, is obtained as [52]

$$p_{LZT} = exp\left(-\frac{\Delta^2}{hv}\right). \quad (1)$$

Here v is the energy sweeping velocity (the time slope of the energy difference between the two states), and h is the Planck constant (details see supplementary note 6). [23] (see also reference [53] therein) The classical LZT has recently received renewed interest in precise control of the quantum states. Figure 3(c) and (d) display the comparison of the amount of nonadiabatic excited electrons predicted by the LZT formula and direct rt-TDDFT simulations (Δ in the former is obtained from the latter), respectively. Interesting enough, we find an excellent agreement in results between the LZT formula and direct rt-TDDFT simulations at low lattice temperature (T < 100 K) or at high initial kinetic energy (E_k > 1 eV). However, at higher temperature (T > 100 K) or low initial kinetic energy (E_k < 1 eV), the LZT results are much larger than that obtained from direct rt-TDDFT simulations. It has also been demonstrated that a two-level quantum system can also be influenced by its coupling to environment [54,55], e.g., due to the thermal phonon mode vibration during the transition period, beyond the classical LZT. The deviation of LZT results from rt-TDDFT indicates the strength of the environmental coupling, which depends on the lattice temperature and impurity passing velocity through the H-site via electron-phonon coupling. Our system provides an excellent opportunity to study this environmental influence. We can deduce that the "dynamic donor" effect is most significant at high lattice temperature but the initial impurity kinetic energy E_k is as small as the diffusion barrier of 0.33 eV, in consistent with direct rt-TDDFT simulations (Fig. 3 and supplementary Fig. S8).

In conclusion, a "dynamic donor" phenomenon during impurity diffusion in Si crystal is revealed by performing rt-TDDFT simulations. We found that, even in the thermally induced low energy impurity diffusion process, the nonadiabatic effect can play a critical role. During the diffusion, the system can pump one electron from an in-gap localized impurity state into the host conduction band, hence loses this electron temporarily, and makes the otherwise neutral impurity into positively charged ion. This happens for Au, Cd and Zn diffusion in Si, as well as for

interstitial Ti diffusion in TiO_2 (see supplementary Fig. S9). We thus believe the "dynamic donor" is a rather common phenomenon. This "dynamic donor" effect can fundamentally change the diffusion process description from the classical ground state transition barrier picture. It reveals that the diffusion process can be a rather complicated process, cannot be understood by studying the nuclei movement alone, and the charge state of an impurity can also change dynamically, and cannot be purely relied on the static ground state calculations. We believe our finding can open up a new direction of inquiring for such fascinating behavior. Secondly, the dynamic donor effect should yield an increase in carrier concentration with temperature. Unfortunately, such dynamic donor-induced increase in carrier concentration overlaps highly with the well-documented fact of the thermally generated intrinsic carriers. At very high temperatures, above 500 K, electrons from the valence band receive enough energy to make it to the conduction band and outnumber the electrons from the donor sites and the majority carrier concentration is now made up of electrons from the valence band in the conduction band, as in an intrinsic semiconductor. New experimental techniques are required to distinguish these two contributions to enhancement in carrier concentration. Finally, our analysis with the rt-TDDFT results provides an excellent example to understand the LZT with environmental effects in a real material. We like to point out that these findings are also relevant to the ion implantation, which is now one of the main processes in the fabrication of modern electronic and optoelectronic devices. The ion diffusion is obviously critical to the implantation process.

Acknowledgments:

L.W.W. was supported by the Director, Office of Science (SC), Basic Energy Science (BES), Materials Science and Engineering Division (MSED), of the US Department of Energy (DOE) under Contract No.DE-AC02-05CH11231 through the Materials Theory program (KC2301). The work in China was supported by the National Natural Science Foundation of China (NSFC) under Grant No. 61888102.

Reference:

[1] S. Pisana, M. Lazzeri, C. Casiraghi, K. S. Novoselov, A. K. Geim, A. C. Ferrari and F. Mauri, Nat. Mater. **6**, 198 (2007).

[2] N. Shenvi, S. Roy and J. C. Tully, Science **326**, 829 (2009).

[3] M. Blanco-Rey, J. I. Juaristi, R. Díez Muiño, H. F. Busnengo, G. J. Kroes, and M. Alducin, Phys. Rev. Lett. **112**, 103203 (2014).

[4] O. Bünermann, H. Y. Jiang, Y. Dorenkamp, A. Kandratsenka, S. M. Janke, D. J. Auerbach and A. M. Wodtke, Science **350**, 1346 (2015).

[5] S. P. Rittmeyer, J. Meyer, J. I. Juaristi and K. Reuter, Phys. Rev. Lett. **115**, 046102 (2015).

[6] S.P. Rittmeyer, D.J. Ward, P. Gutlein, J. Ellis, W. Allison and K. Reuter, Phys. Rev. Lett. **117**, 196001 (2016).

[7] R. J. Maurer, B. Jiang, H. Guo and J. C. Tully, Phys. Rev. Lett. **118**, 256001 (2017).

[8] S. P. Rittmeyer, J. Meyer and K. Reuter, Phys. Rev. Lett. **119**, 176808 (2017).

[9] A. V. Krasheninnikov, Y. Miyamoto and D. Tomanek, Phys. Rev. Lett. **99**, 016104 (2007).

[10] R. Hatcher, M. Beck, A. Tackett and S. T. Pantelides, Phys. Rev. Lett. **100**, 103201 (2008).

[11] S. N. Markin, D. Primetzhofer and P. Bauer, Phys. Rev. Lett. **103**, 113201 (2009).

[12] A. A. Correa, J. Kohanoff, E. Artacho, D. Sanchez-Portal and A. Caro, Phys Rev Lett. **108**, 213201 (2012).

[13] M. A. Zeb, J. Kohanoff, D. Sanchez-Portal, A. Arnau, J. I. Juaristi and E. Artacho, Phys. Rev. Lett. **108**, 225504 (2012).

[14] R. Ullah, F. Corsetti, D. Sánchez-Portal, E. Artacho, Phys. Rev. B **91**, 125203 (2015).

[15] Y. W Zhang, R. Sachan, O. H. Pakarinen, M. F. Chisholm, P. Liu, H. Z. Xue and W. J. Weber, *Nat. Commun.* **6**, 8049 (2015).

[16] A. Lim, W. M. Foulkes, A. P. Horsfield, D. R. Mason, A. Schleife, E. W. Draeger and A. A. Correa, Phys. Rev. Lett. **116**, 043201 (2016).

[17] E. E.Quashie, B. C. Saha and A. A. Correa, Phys. Rev. B **94**, 155403 (2016).

[18] D. Roth, B. Bruckner, M. V. Moro, S. Gruber, D. Goebl, J. I. Juaristi, M. Alducin, R. Steinberger, J. Duchoslav, D. Primetzhofer, and P. Bauer, Phys. Rev. Lett. **118**, 103401 (2017).

[19] N. E. B. Cowern, S. Simdyankin, C. Ahn, N. S. Bennett, J. P. Goss, J. M. Hartmann, A. Pakfar, S. Hamm, J. Valentin, E. Napolitani, D. De Salvador, E. Bruno and S. Mirabella, Phys. Rev. Lett. **110**,155501 (2013).

[20] T. Südkamp, H. Bracht, Phy. Rev. B **94**, 125208 (2016).

[21] Z. Wang, S. S. Li and L. W. Wang, Phys. Rev. Lett. **114**, 063004 (2015).

[22] M. Trochet, L. K. Béland, J. F. Joly, P. Brommer and N. Mousseau, Phys. Rev. B **91**, 224106 (2015).

[23] See Supplemental Material at [xxx], which includes Refs. [47, 48, 52], for supplemental results and discussions.

[24] W. L. Jia, Z. Y. Cao, L. Wang, J. Y. Fu, X. B. Chi, W. G. Gao and L. W. Wang, Computer Physics Communications **184**, 9 (2013).

[25] M. R. Provorse and C. M. Isborn, *International Journal of Quantum Chemistry* **116**, 739 (2016).

[26] G. Kolesov, O. Granas, R. Hoyt, D. Vinichenko and E. Kaxiras, J. Chem. Theory. Comput. **12**, 466 (2016).

[27] T. Ziegler, A. Rank, and E. J. Baerends, Theoret. Chim. Acta (Berl.) **43**, 261 (1977).

[28] Computational Chemistry: A Practical Guide for Applying Techniques to Real World Problems, by David Young (Wiley-Interscience, New York 2001).

[29] G. Kolesov, B. A. Kolesovand E. Kaxiras, Phys Rev. B **96**, 195165 (2017).

[30] M. M. Montemore, R. Hoyt, G. Koleso and E. Kaxiras, *ACS Catal*. **8**, 10358 (2018).

[31] R. A. Hoyt, M. M. Montemore and E. Kaxiras, J. Phys. Chem. Lett. **9**, 5339 (2018).

[32] S. K. Estreicher, D. J. Backlund, C. Carbogno and M. Scheffler, Angew. Chem. Int. Ed. Engl. **50**, 10221 (2011).

[33] J. Ma and S. H. Wei, Phys. Rev. Lett. **110**, 235901 (2013).

[34] J. H. Yang, J. S. Park, J. Kang and S. H. Wei, Phys. Rev. B **91**, 075202 (2015).

[35] R. Brunetti, C. Jacoboni, F. Nava, L. Reggiani, G. Bosman and R. J. J. Zijlstra, Journal of Applied Physics, 52, 6713 (1981).

[36] S. K. Cushing, M. Zurch, P. M. Kraus, L. M. Carneiro, A. Lee, H. T. Chang, C. J. Kaplan, S. R. Leone, Struct Dyn. 5, 054302 (2018).

[37] C. J. Gallagher, Phys. Chem. Solids **3**, 82 (1957).

[38] E. R. Weber, Appl. Phys. A **30**, 1 (1983).

[39] A. A. Istratov, C. Flink, H. Hieslmair and E. R. Weber, Phys. Rev. Lett. **81**, 1243 (1998).

[40] F. J. H. Ehlers, A. P. Horsfield and D. R. Bowler, Phys. Rev. B **73**, 165207 (2006).

[41] H. X. Deng, J. W. Luo, S. S. Li and S. H. Wei, Phys. Rev. Lett. **117**, 165901 (2016).

[42] A. Sharan, Z. Gui and A. Janotti, Phys. Rev. Applied **8**, 024023 (2017).

[43] C. S. Fuller and J. C. Severiens, Phys. Rev. **96**, 21 (1954).

[44] C. U. Saguy, C. Cytermann, B. Fizgeer, V. Richter, R. Brener and R. Kalish, phys. stat. sol. (a) **193**, 508 (2002).

[45] V. Meunier, J. Kephart, C. Roland and J. Bernholc, Phys. Rev. Lett. **88**, 075506 (2002).

[46] G. Luo, T. F. Kuech and D. Morgan, NPG Asia Materials **10**, 45 (2018).

[47] C. Freysoldt, B. Grabowski, T. Hickel, J. Neugebauer, G. Kresse, A. Janotti and C. G. Van de Walle, Rev. Mod. Phys. 86, 253 (2014).

[48] P. A. Schultz, Phys. Rev. B 93, 125201 (2016).

[49] J. W. Chen and A. G. Milnes, Ann. Rev. Mater. Sci. **10**, 157 (1980).

[50] A. Fazzio, M. J. Caldas and A. Zunger, Phys. Rev. B **32**, 934 (1985).

[51] S. W. Jones, Diffusion in Silicon, IC Knowledge LLC (2008).

[52] C. Zener, Proc. R. Soc. A **137**, 696 (1932).

[53] Y. Kayanuma and H. Nakayama, Phys. Rev. B, **57**, 13099 (1998).

[54] P. Nalbach and M. Thorwart, Phys. Rev. Lett. **103**, 220401 (2009).

[55] S. S. Zhang, W. Gao, H. Cheng, L. You and H. P. Liu, Phys. Rev. Lett. **120**, 063203 (2018).

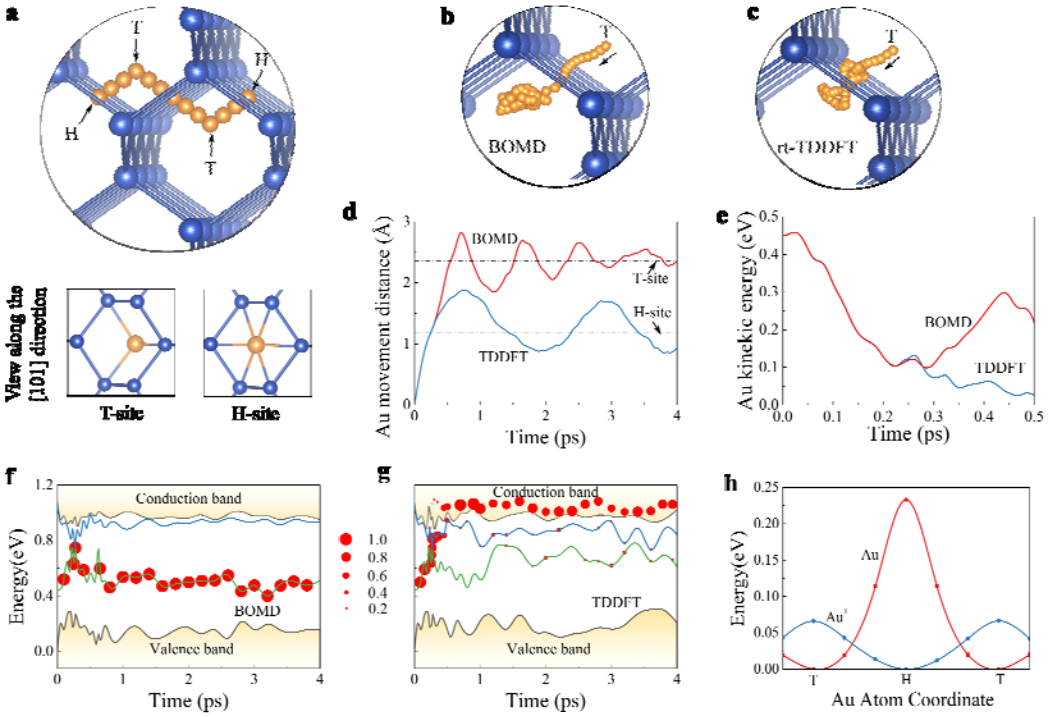

FIG. 1. (a) The diffusion path of interstitial Au atom along the <111> direction. The big blue balls represent Si atoms, and the small orange balls track the trajectory of the interstitial Au atom. The high symmetry sites such as Tetrahedral site (T-site) and Hexagonal site (H-site) are marked. (b) and (c) The diffusion trajectory of Au impurity in the BOMD and TDDFT simulations when the initial kinetic E_k (t_0) = 0.45 eV. (d) and (e) The corresponding Au impurity movement distance and kinetic energy as a function of time. (f) and (g) Evolution of adiabatic state energy levels as functions of time in BOMD and rt-TDDFT simulations. Green (blue) lines represent the impurity level-1 (level-2) inside the Si band gap. Red solid circles indicate the occupations of the impurity electron with its size represents the amplitude of the occupation. (h) The PES along the diffusion path of Au and Au^+ based on NEB method. Here, we set the minimum energy of the PES to zero.

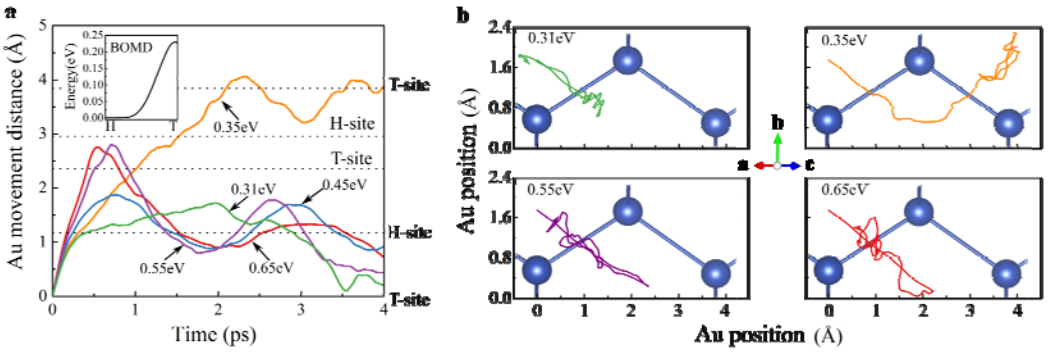

FIG. 2. (a) Au atom movement distance away from the initial position at T-site as a function of time for different initial kinetic energy E_k = 0.31, 0.35, 0.45, 0.55 and 0.65eV under temperature T = 550 K based on the rt-TDDFT simulations. Inset shows the kinetic energy of Au atom from H-site to T-site based on BOMD simulation. (b) Au atom movement trajectory along <$\bar{1}$01> (x-axis) and <010> (y-axis) direction.

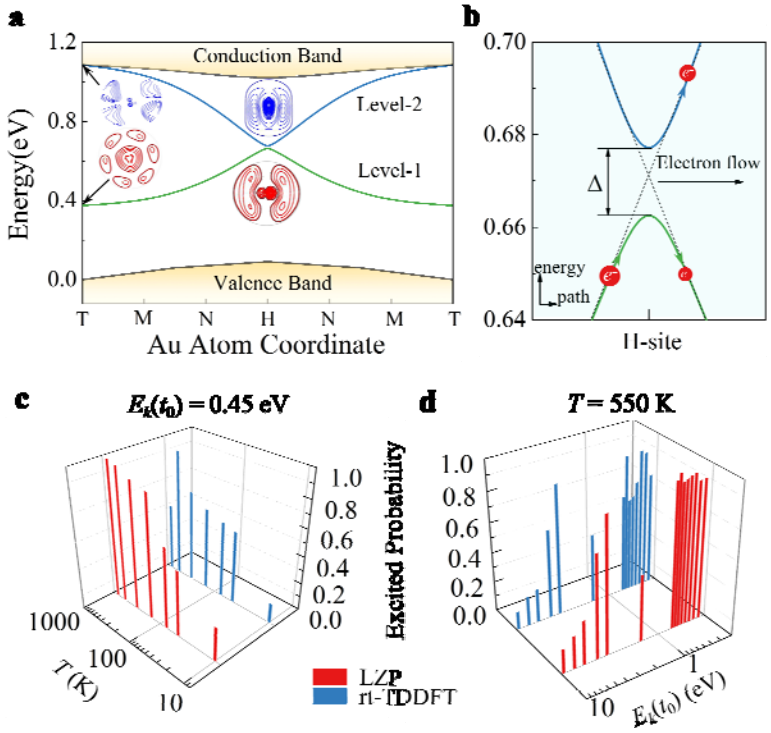

FIG. 3. (a) Evolution of eigenvalues at the supercell Γ-point as the interstitial Au impurity moves away from its initial T-site based on the DFT calculation. The diffusion path of Au atom, from T-site through H-site to T-site along the <111> direction, and M and N are two points between T- and H-sites along the path. Green (blue) lines represent the impurity level 1 (level-2) in the Si band gap. The insets are the wave functions of two impurity states for Au at T- and H-sites, respectively. (b) The schematic diagram for two anticrossing levels around the H-site with a gap of Δ. (c) and (d) Comparison of the excited electrons between the rt-TDDTF simulations (blue bars) and classic LZT (red bars) for fixed initial kinetic energy to 0.45 eV but different temperature and fixed temperature to 550 K but different initial kinetic energies, respectively.